Available online at www.sciencedirect.com
SCIENCE DIRECT®
Journal of Power Sources 148 (2005) 105–111
JOURNAL OF POWER SOURCES
www.elsevier.com/locate/jpowsour

Effect of substituting Co with Fe on the cycle stabilities of the as-cast and quenched AB_5-type hydrogen storage alloys

Yang-Huan Zhang [a,b,*], Guo-Qing Wang [a], Xiao-Ping Dong [b], Shi-Hai Guo [a], Jiang-Yuan Ren [b], Xin-Lin Wang [a]

[a] *Department of Functional Material Research, Central Iron and Steel Research Institute, 76 Xuanyuannan Road, Haidian District, Beijing 100081, China*
[b] *School of Material, Inner Mongolia University of Science and Technology, Baotou 014010, China*

Received 6 December 2004; received in revised form 26 January 2005; accepted 1 February 2005
Available online 11 April 2005

Abstract

The rare-earth-based AB_5-type $Mm(NiMnSiAl)_{4.3}Co_{0.6-x}Fe_x$ ($x = 0$, 0.1, 0.2, 0.3, 0.4, 0.5, 0.6) hydrogen storage alloys were prepared by casting and rapid quenching. The microstructures of the as-cast and quenched alloys were analysed by XRD, SEM and TEM, and electrochemical cycle stabilities of the alloys were measured. The effects of substituting Co with Fe on microstructures and cycle stabilities of the as-cast and quenched alloys were investigated in detail. The obtained results show that the effects of substituting Co with Fe on the phase structures of the as-cast and quenched alloys are imperceptible, but its effects on cycle stabilities of the alloys are notable. Substituting Co with Fe improves slightly the cycle stabilities of the as-cast alloys, but it can significantly enhance the cycle lives of the as-quenched alloys, which is mainly attributed to the grain refinement of the alloys caused by substituting Co with Fe.
© 2005 Elsevier B.V. All rights reserved.

Keywords: Substituting Co with Fe; AB_5-type hydrogen storage alloy; As-cast and quenched; Microstructure; Cycle stability

1. Introduction

Ni–MH batteries have been using widely by virtue of several of their advantages, such as high capacity, high resistance to overcharging and over-discharging, capable of performing a high rate charge/discharge, environmental friendliness, and interchangeability with Ni–Cd batteries. AB_5-type hydrogen storage alloy has realized large-scale industrialization in many countries, especially in Japan, USA and China [1,2]. In the very recent years, however, the rechargeable Ni–MH cells are facing serious challenge owing to quick development of Li-ion cells. On the one hand, the Li-ion cells show higher energy density than the Ni–MH cells per unit weight or volume. On the other hand, the production cost of Ni–MH battery based on the current technology also limits its widespread applications because low-cost Pb-acid batteries are still dominating the sector. For the negative electrode materials of Ni–MH battery, the discharge capacity of the current advanced AB_5-type alloys has reached 310–330 mAh g^{-1}. Therefore, further improvement on the capacity of AB_5-type alloys seems to be very difficult since the theoretical capacity of $LaNi_5$ is about 372 mAh g^{-1}. In order to broaden application field of Ni–MH batteries and enhance their competition ability, a realistic approach is to reduce the production cost of hydrogen storage alloy [3–11]. Although researchers have done much work for preparing low-Co and Co-free AB_5-type hydrogen storage alloys around the world, the obtained results are still unsatisfactory [7,9]. The main problem is that the cycle stabilities of low-Co and Co-free AB_5-type electrode alloys are poor because the function of Co on the cycle stability of AB_5-type hydrogen storage alloy is extremely important [12]. In order to improve the cycle stabilities of low-

* Corresponding author. Tel.: +86 10 62187570; fax: +86 10 62182296.
E-mail addresses: zyh59@yahoo.com.cn, zhangyh59@163.com (Y.-H. Zhang).

0378-7753/$ – see front matter © 2005 Elsevier B.V. All rights reserved.
doi:10.1016/j.jpowsour.2005.02.004

Co and Co-free hydrogen storage alloys, multi-component AB_5-type hydrogen storage alloy with single phase or two-phase structure have been prepared by rapid quenching in our previous research [13,14], and investigation results show that low-Co and Co-free AB_5-type hydrogen storage alloys with good synthetic electrochemical performances can be prepared by scientific composition design and using suitable rapid quenching technique. The paper studied the effect of substituting Co with Fe on the microstructures and electrochemical cycle stabilities of the as-cast and quenched $Mm(NiMnSiAl)_{4.3}Co_{0.6-x}Fe_x$ ($x = 0$, 0.1, 0.2, 0.3, 0.4, 0.5, 0.6) hydrogen storage alloys, and obtained some valuable results.

2. Experimental

2.1. Alloy preparation

The alloys were melted with an induction furnace in an argon atmosphere. The melt was poured into a copper mould cooled by water, and a cast ingot was obtained. Part of the as-cast alloys was re-melted and quenched by melt-spinning with a rotating copper wheel, obtaining flakers of as-quenched alloy with quenching rates of 10, 16, 22, 28 m s^{-1}. The quenching rate was expressed by the linear velocity of the copper wheel. The chemical compositions of the experimental alloys are $Mm(NiMnSiAl)_{4.3}Co_{0.6-x}Fe_x$ ($x = 0$, 0.1, 0.2, 0.3, 0.4, 0.5, 0.6). Corresponding with Fe content x, the alloys are represented with Fe_0, Fe_1, Fe_2, Fe_3, Fe_4, Fe_5 and Fe_6. The purity of all the component metals (Ni, Co, Mn, Si, Al, Fe) is at least 99.7%. Mm denotes Ce-rich Mischmetal (23.70 wt.% La, 55.29 wt.% Ce, 5.31 wt.% Pr, 15.70 wt.% Nd) with the purity of 99.85%.

2.2. Electrode preparation and electrochemical measurement

The fractions of the as-cast and quenched alloys, which were ground mechanically into powder below 250 meshes, were used for the preparation of the experimental electrode. Electrode pellets with 15 mm diameter were prepared by mixing 1 g alloy powder with fine nickel powder in a weight ratio of 1:1 together with a small amount of polyvinyl alcohol (PVA) solution as binder, and then compressed under a pressure of 35 MPa. After drying for 4 h, the electrode pellets were immersed in 6 M KOH solution for at least 24 h in order to wet fully the electrodes before the electrochemical measurement.

The experimental electrodes were tested in a tri-electrode open cell, consisting of a working electrode (metal hydride electrode), a counter electrode ($NiOOH/Ni(OH)_2$) and a reference electrode (Hg/HgO). In order to reduce the ohmic drop between the working electrode and the reference electrode, a Luggin capillary was located close to the hydride electrode in the working electrode apartment. The electrolyte was a 6 M KOH solution. The cycle life was measured by an automatic galvanostatic charge–discharge unit (30 °C). Every cycle was overcharged to about 30% with constant current of 300 mA g^{-1} after a 15 min pause. The discharge cut-off potential is −0.5 V versus Hg/HgO reference electrode.

2.3. Microstructure determination and morphology observation

The samples of the as-cast alloys were directly polished and flakes of the as-quenched alloys were inlaid in epoxy resin for polishing. The samples thus prepared were etched with a 60% HF solution. The morphologies of the as-cast and quenched alloys were observed by SEM. The samples of the as-cast and quenched alloys were pulverized by mechanical grinding, getting the power samples with the size less than 50 μm. The phase structures and lattice parameters of the as-cast and quenched alloys were determined by X-ray diffractometer of *D*/max/2400. The diffraction was performed with Cu $K\alpha_1$ diffraction filtered by graphite. The experimental parameters for determining phase structure were 160 mA, 40 kV and 10° min^{-1}, respectively. The powder samples were dispersed in anhydrous alcohol for observing the grain morphology with TEM and determining crystal state with SAD. The granular morphologies of the alloy electrode before and after electrochemical cycle were observed by SEM in order to reveal the mechanism of the efficiency loss of the alloy electrode.

3. Results and discussion

3.1. Electrochemical cycle stability

The cycle number dependence of the discharge capacities of the as-cast and quenched alloys is illustrated in Fig. 1. It can be derived from Fig. 1 that substituting Co with Fe decreases slightly the slopes of curves corresponding with the as-cast alloys. It indicates that substituting Co with Fe improves the cycle stabilities of the as-cast alloys. For the as-quenched (22 m s^{-1}) alloys, the slopes of the curves decrease in the beginning and then increase with the increase of the amount of substituting Co with Fe. It can be concluded that the cycle stability of the as-quenched alloy is not linear with the Fe content.

In order to evaluate accurately the cycle stability of the alloys, two definitions, capacity retaining rate and capacity decay rate, are introduced. The capacity retaining rate denoted by R_h is defined as $R_h = \frac{C_{300,300}}{C_{300,max}} \times 100\%$, where $C_{300,max}$ is the maximum discharge capacity with a charge–discharge current density of 300 mA g^{-1}, and $C_{300,300}$ the discharge capacity at 300th cycles, respectively. The capacity decay rate denoted by D is defined as $D = \frac{C_{300,max} - C_{300,300}}{300-n} \times 100\%$, where n is activation number. According to the above-mentioned definitions, it can be known that the larger the

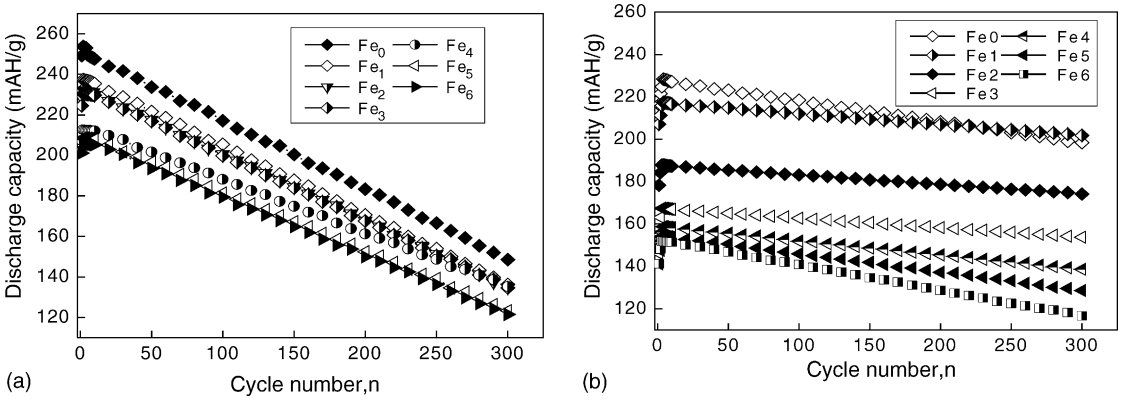

Fig. 1. The relationship between cycle number and discharge capacity of the as-cast and quenched alloys (22 m s^{-1}): (a) as-cast; (b) as-quenched.

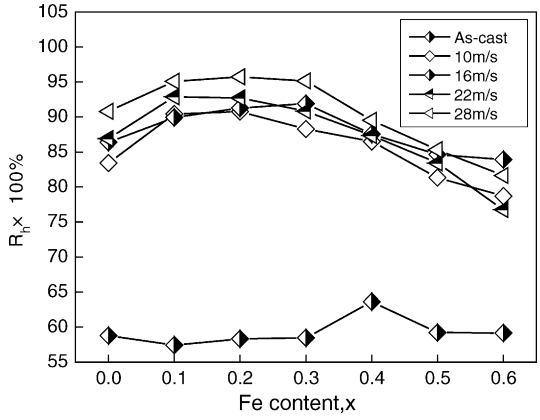

Fig. 2. The relationship between the Fe content and the capacity retaining rate (R_h).

capacity retaining rate (R_h), the smaller the capacity decay rate (D), and the better the cycle stability of the alloy. The Fe content dependence of the capacity retaining rates and the capacity decay rates of the as-cast and quenched alloys is illustrated in Figs. 2 and 3, respectively. Fig. 2 indicates that substituting Co with Fe can enhances capacity retaining rates of the as-cast alloys slightly and a maximum R_h of the as-quenched alloy can be obtained with the variety of Fe content. A similar result can be obtained in Fig. 3.

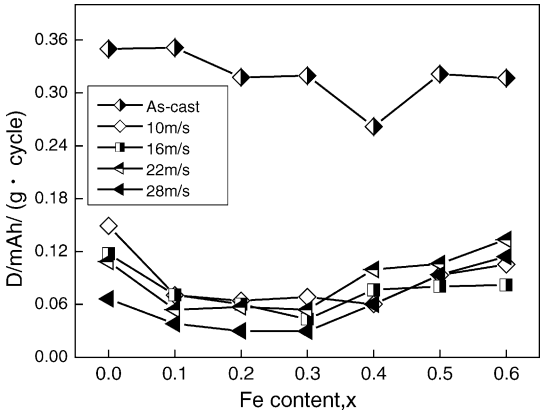

Fig. 3. The relationship between the Fe content and the capacity decay rate (D).

3.2. Microstructure

3.2.1. Microstructure morphology

The microstructure morphologies of the as-cast alloys were observed by SEM, and the results were illustrated in Fig. 4. Fig. 4 shows that the grain sizes of the as-cast alloys are very large and the homogeneity of the compositions of the as-cast alloys is very poor. The results of microzone energy spectrum analysis with SEM, which were listed in Table 1, show that the as-cast alloys are composed of Mm-rich main-phase (deep gray regions) and Ni-rich main phase (shallow gray regions) as well as a trace of Ce_2Ni_7 phase (small white regions). The morphologies and distributions of Mm-rich and Ni-rich phase vary with the increase of the amount of substituting Co with Fe. It displays that the concentration distribution of Mm-rich phase is changed into dispersion distribution with the increase of the amount of substituting Co with Fe. The reason for the presence of Ce_2Ni_7 phase is that the composition of the alloys is non-stoichiometric. The longitudinal section morphologies of the as-quenched alloys with a quenching rate of 22 m s^{-1} were observed by SEM and the results were illustrated in Fig. 5. It can be concluded by comparing Fig. 4 with Fig. 5 that rapid quenching can result in the refining of the grain of the alloy and the uniforming of the composition of the alloy. It also can be derived from Fig. 5 that the grain of the as-quenched alloys is markedly refined with the increase of the Fe content although the same rapid quenching technology is used. The mechanism of substituting Co with Fe refining grains of the as-quenched alloys needs to be investigated further. The microstructure morphologies of the as-quenched alloys were observed by TEM and crystalline states of the as-quenched alloys were determined with SAD. The results were illustrated in Fig. 6. The results obtained by SAD indicate that the as-quenched Fe_0 and Fe_4 alloys with quenching rate of 22 m s^{-1} have an obvious tendency to form amorphous phase, and a certain amount of the

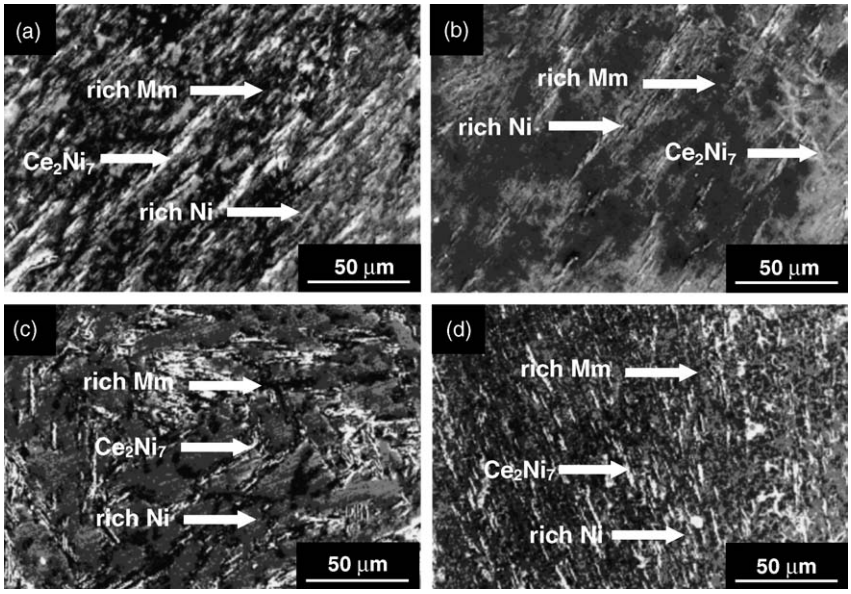

Fig. 4. The morphologies of the as-cast alloys (SEM): (a) Fe_0; (b) Fe_2; (c) Fe_4; (d) Fe_6.

Table 1
The compositions of the main phases of the as-cast alloys (at.%)

Alloys	Main phases	Mm	Ni	Mn	Al	Si	Co	Fe	Fe/Co
Fe_0	Rich Mm	17.93	56.55	7.13	4.17	1.98	12.21	0	–
	Rich Ni	15.38	67.73	5.26	1.94	0.86	8.54	0	–
Fe_2	Rich Mm	17.25	57.32	6.95	3.98	2.01	8.31	4.17	0.50
	Rich Ni	15.02	68.12	5.31	2.28	0.87	5.38	2.94	0.55
Fe_4	Rich Mm	17.31	56.31	7.52	3.74	2.01	4.57	8.44	1.85
	Rich Ni	14.97	69.04	4.18	2.13	1.02	2.91	5.66	1.94
Fe_6	Rich Mm	17.58	55.83	8.46	3.68	2.13	0	12.24	–
	Rich Ni	14.71	70.12	40.60	2.73	0.91	0	7.44	–

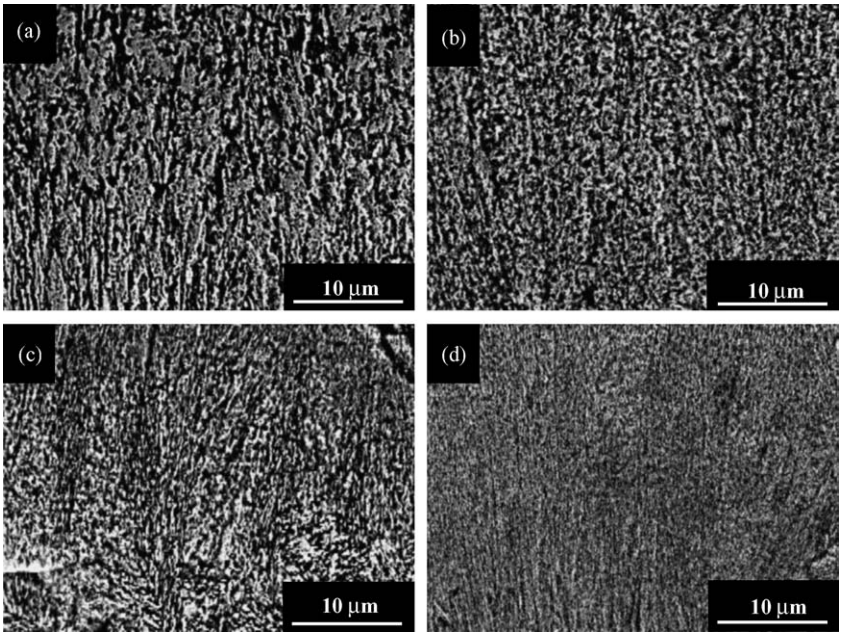

Fig. 5. Longitudinal section morphologies of the as-quenched (22 m s^{-1}) alloys taken by SEM: (a) Fe_0; (b) Fe_2; (c) Fe_4; (d) Fe_6.

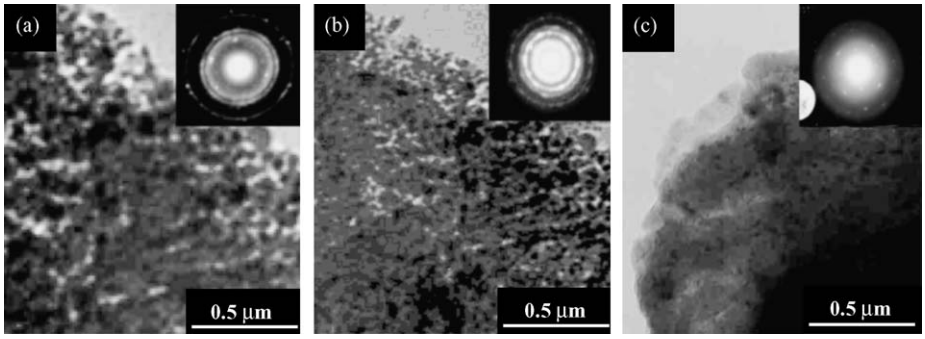

Fig. 6. The morphologies and SAD of the as-quenched alloys (22 m s^{-1}) (TEM): (a) Fe_0; (b) Fe_4; (c) Fe_6.

amorphous phase existed in the as-quenched Fe_6 alloy with quenching rate of 22 m s^{-1}.

3.2.2. Phase composition and structure

The phase composition and structure of the as-cast and quenched alloys were determined by XRD. The X-ray diffraction patterns of the as-cast and quenched alloys are illustrated in Fig. 7. It can be seen from Fig. 7 that the as-cast alloys have a two-phase structure composed of a $CaCu_5$-type main phase and a small amount of Ce_2Ni_7-type secondary phase. The effect of substituting Co with Fe on the two-phase structures is insignificant. After the alloys are quenched with the rate of 22 m s^{-1}, the amount of Ce_2Ni_7 secondary phase decreases obviously. It can be seen from Fig. 7(b) that the intensity of the diffraction peaks of the as-quenched alloys with different composition are basically uniform. This shows that the crystalline orientation of the as-quenched alloys is more homogeneous. The lattice constants of the as-cast and quenched alloys were calculated from the diffraction peaks of (1 0 1), (1 1 0), (2 0 0), (1 1 1) and (0 0 2) crystal planes of the main phase of the alloys by a method of least squares and the cell volumes of the alloys were calculated with formula $V = a^2 c \sin 60°$. The calculated results are listed in Table 2. It can be derived from Table 2 that the lattice constants and cell volumes of the alloys slightly increased with the increase of the Fe content.

The effect of substituting Fe with Co on the cycle stability of the as-quenched alloys includes two favourable and unfavourable aspects. The grain refinement and the increase of the cell volume resulted from substituting Fe with Co is favourable, but the decrease of anti-corrosion ability produced by substituting Fe with Co is unfavourable. Therefore, it is certain that the capacity retaining rate R_h of the as-quenched alloy have a maximum value with the variety of the amount of substituting Fe with Co.

The cycle stability of the electrode alloy is a decisive factor of the life of Ni–MH battery. The root cause of leading to the efficacy loss of battery is on negative electrode rather than on positive electrode. The battery failure is characterized by a decay of the discharge capacity and a decrease

Table 2
Lattice constants and cell volumes of the main phase in the as-cast and quenched alloys

Alloy	Lattice constants				Cell volumes	
	a (Å)		c (Å)		V (Å)^3	
	As-cast	22 m s^{-1}	As-cast	22 m s^{-1}	As-cast	22 m s^{-1}
Fe_0	4.99	4.97	4.05	4.06	87.41	87.42
Fe_2	5.01	4.99	4.06	4.06	88.19	87.72
Fe_4	5.01	5.02	4.07	4.07	88.65	88.79
Fe_6	5.02	5.02	4.08	4.07	89.11	88.75

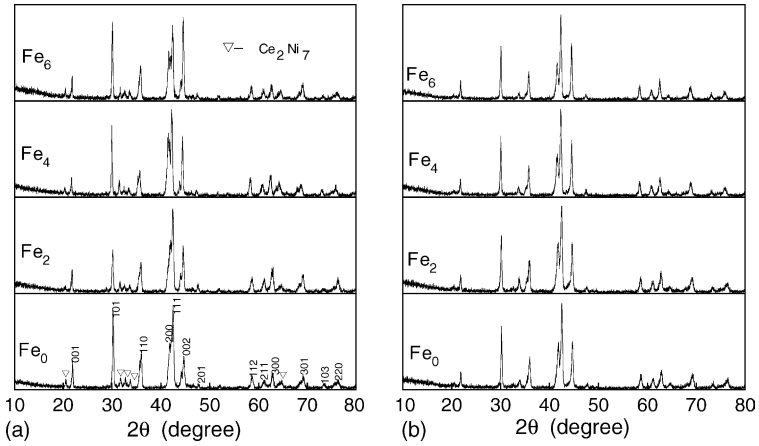

Fig. 7. The X-ray diffraction patterns of the as-cast and quenched alloys: (a) as-cast; (b) as-quenched (22 m s^{-1}).

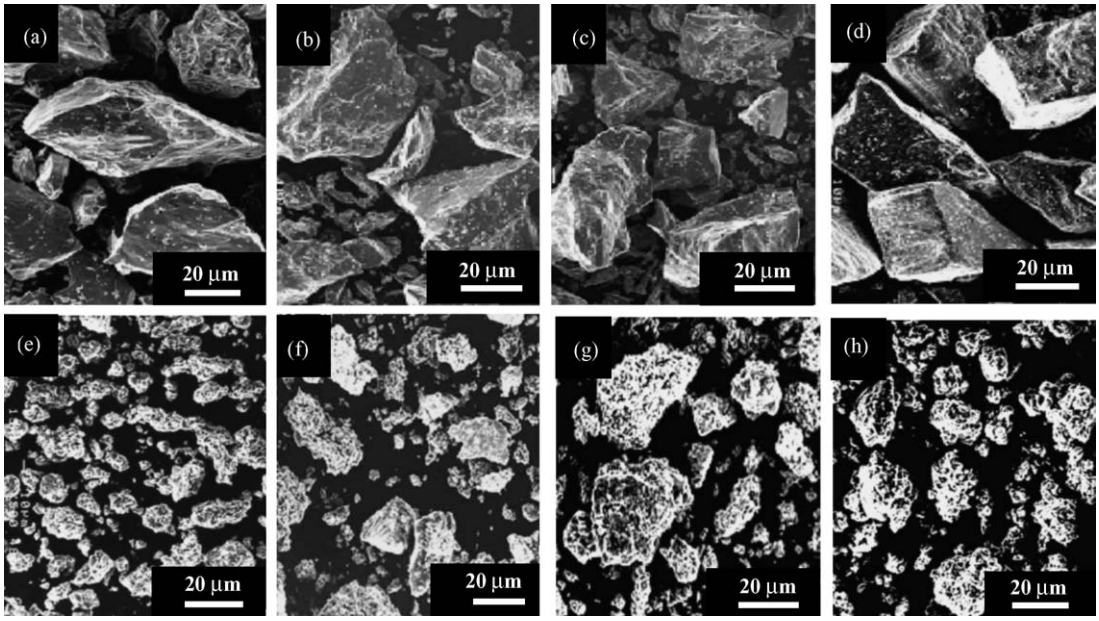

Fig. 8. The granular morphologies of as-cast alloys before and after electrochemical cycle (SEM): (a–d) before cycle of Fe_0, Fe_2, Fe_4 and Fe_6; (e–h) after cycle of Fe_0, Fe_2, Fe_4 and Fe_6.

of the discharge voltage. It is confirmed in the literature [15–17] that the fundamental reasons for the capacity decay of the electrode alloy are the pulverization and oxidation of the alloy during charge–discharge cycle. The lattice internal stress and cell volume expansion, which are inevitable when hydrogen atoms enter into the interstitials of the lattice, are the real driving force that leads to the pulverization of the alloy. The reason for substituting Co with Fe enhancing the cycle life of the as-cast alloys is mainly attributed to the substituting Co with Fe leading to homogeneous distribution of Mm-rich main phase. Obviously, the uniformity of structure and composition can enhance the cycle stability of the alloy. The main cause of the substituting Co with Fe enhancing the cycle stability of the as-quenched alloy is the grain refinement produced by substituting Co with Fe. The determining factors of the cycle life of the alloy are its anti-pulverization and oxidation capabilities. The smaller the grain size of the alloy, the higher the strength and toughness, and the stronger the anti-pulverization capability. The morphologies of the as-cast Fe_0, Fe_2, Fe_4 and Fe_6 alloys particles before and after electrochemical cycle taken by SEM are shown in Fig. 8. Fig. 8 shows that the shapes of the alloy particles before electrochemical cycle are irregular and sharp-angled. This is characteristic of mechanical pulverization. After the Fe_0, Fe_2, Fe_4 and Fe_6 alloys passed 245, 244, 364 and 325 charge–discharge cycles, respectively, the morphologies of alloy particles changed markedly, leading to the cracking of the alloy particles. The main reason of leading to the capacity decay is the pulverization of the alloy during absorbing and desorbing hydrogen. Worthy of remark is that cycle number of the Fe_4 and Fe_6 alloys is 119 and 80 cycles larger than that of the as-cast Fe_0 alloy, respectively. Whereas the particle sizes of the Fe_4 and Fe_6 alloys are still larger than that of the Fe_0 alloy. Therefore, it can be concluded that anti-pulverization capability of the alloy can be improved by substituting Co with Fe. It can be derived from the morphologies of the Fe_0, Fe_2, Fe_4 and Fe_6 alloys particles before and after electrochemical cycle that the particle sizes of the Fe_2, Fe_4 and Fe_6 alloys are obviously larger than that of Fe_0 alloy when discharge capacities of the alloys are reduced to 60% of their maximum capacity. It shows that substituting Co with Fe improves the anti-pulverization capability of the as-cast alloy, but decreases the anti-corrosion capability of the alloy in alkaline electrolyte. Therefore, it can be concluded that the main cause of leading to the efficacy loss of the electrode alloy is its pulverization during charge–discharge cycle, and corrosion and oxidation of the alloy is also important factors.

4. Conclusion

1. Substituting Co with Fe has an insignificant influence on the phase composition and structure of the as-cast and quenched $Mm(NiMnSiAl)_{4.3}Co_{0.6-x}Fe_x$ ($x = 0$, 0.1, 0.2, 0.3, 0.4, 0.5, 0.6) hydrogen storage alloys, but it changes the phase distribution and microstructure morphologies of the alloys. For the as-cast alloys, the concentration distribution of Mm-rich phase is changed into dispersion distribution with the increase of the amount of substituting Co with Fe. And for the as-quenched alloys, the grain of the alloys is markedly refined with the increase of the Fe content. The lattice constants and cell volumes of the as-cast and quenched alloys slightly increased with the increase of the Fe content.
2. Substituting Co with Fe improves the electrochemical cycle stability of the alloy, especially greatly improves the

cycle life of the as-quenched alloy, but the cycle life of the alloy is not linear with the Fe content. The optimal Fe content is relevant to the composition of the alloy. For the composition of the alloys in our experiment, the suitable amount of substituting Co with Fe is $x \leq 0.4$.

3. The main cause of leading to the efficacy loss of the electrode alloy is its oxidation and pulverization during charge–discharge cycle. Substituting Co with Fe improves the anti-pulverization capability of the alloy in process of absorbing and desorbing hydrogen, but decreases the anti-corrosion and oxidation capability of the alloys in alkaline electrolyte.

Acknowledgement

This work is supported by National Natural Science Foundations of China (50131040).

References

[1] I. Uehara, T. Sakai, H. Ishikawa, J. Alloys Compd. 253/254 (1997) 635–641.
[2] Q.D. Wang, C.P. Chen, Y.Q. Lei, J. Alloys Compd. 253/254 (1997) 629–634.
[3] W.-K. Hu, J. Alloys Compd. 279 (1998) 295–300.
[4] P. Li, X.-L. Wang, Y.-H. Zhang, R. Li, J.-M. Wu, X.-H. Qu, J. Alloys Compd. 353 (2003) 278–282.
[5] W.-K. Hu, H. Lee, D.-M. Kim, S.-W. Jeon, J.-Y. Lee, J. Alloys Compd. 268 (1998) 261–265.
[6] P. Li, X.-L. Wang, Y.-H. Zhang, J.-M. Wu, R. Li, X.-H. Qu, J. Alloys Compd. 354 (2003) 310–314.
[7] J.M. Cocciantelli, P. Bernard, S. Fernandez, J. Atkin, J. Alloys Compd. 253/254 (1997) 642–647.
[8] P. Li, Y.-H. Zhang, X.-L. Wang, Y.-F. Lin, X.-H. Qu, J. Power Sources 124 (2003) 285–292.
[9] W.-K. Hu, D.-M. Kim, K.-J. Jang, J.-Y. Lee, J. Alloys Compd. 269 (1998) 254–258.
[10] C. Iwakura, K. Ohkawa, H. Senoh, H. Inoue, J. Electrochem. Soc. 149 (2002) A462–A465.
[11] R. Tang, Y. Liu, J. Zhu, G. Yu, J. Electrochem. Soc. 151 (2004) A1774–A1777.
[12] D. Chartouni, F. Meli, A. Züttel, K. Gross, L. Schlapbach, J. Alloys Compd. 241 (1996) 160–166.
[13] Y.-H. Zhang, M.-Y. Chen, X.-L. Wan, G.-Q. Wang, X.-P. Dong, Y. Qi, Electrochim. Acta 49 (2004) 1161–1168.
[14] Y.-H. Zhang, M.-Y. Chen, X.-P. Dong, G.-Q. Wang, X.-L. Wang, J. Alloys Compd. 376 (2004) 275–281.
[15] T. Sakai, K. Oguro, H. Miyamura, N. Kuriyama, A. Kato, H. Ishikawa, J. Less-Common Met. 161 (1990) 193–202.
[16] A.H. Boonstra, T.M.N. Bernards, J. Less-Common Met. 161 (1990) 355–368.
[17] A.H. Boonstra, T.M.N. Bernards, J. Less-Common Met. 161 (1990) 245–255.